Electronic Supplementary Material (ESI) for Chemical Communications.

Supplementary Information

Insights into Fe-doping effect induced heterostructure formation for oxygen evolution reaction

Xingyu Huang[a], Lice Yu[a], Xinzhong Wang[b], Ligang Feng*[a]

[a] School of Chemistry and Chemical Engineering, Yangzhou University, Yangzhou 225002, P.R. China.

[b] Information Technology Research Institute, Shenzhen Institute of Information Technology, Shenzhen, China

Email: ligang.feng@yzu.edu.cn; fenglg11@gmail.com

Experimental Sections

Chemicals

All chemicals were purchased and used without any additional purification. $Ni(NO_3)_2 \cdot 6H_2O$, $FeCl_3 \cdot 6H_2O$, NH_4F, $CO(NH_2)_2$, CH_3CH_2OH and $C_2H_6O_2$ were bought from Shanghai Aladdin Bio-Chem Technology Co., LTD. KOH was purchased from Sinopharm Chemical Reagent Co., Ltd. All solutions were prepared with ultrapure water (Thermo Fisher Scientific (USA) Co., Ltd). Besides, IrO_2 (99.9%) powders were bought from Shanghai Macklin Biochemical Technology Co., Ltd.

Synthesis of Fe-doped $Ni(OH)_2$ precursor

$Ni(NO_3)_2 \cdot 6H_2O$ (2 mmol), $FeCl_3 \cdot 6H_2O$ (0.1 mmol, 0.2 mmol, 0.3 mmol), NH_4F (10 mmol), and hexamethylenetetramine (HMTA) (1.2 mmol) were dissolved in distilled water (80 mL) with continuous stirring. The obtained solution was transferred into a 200 mL autoclave reactor and maintained at 120 ^oC for 9 h. After being washed with deionized water and absolute ethanol, and dried at 60 ^oC for 6 h, the Fe-doped $Ni(OH)_2$ was obtained.

Synthesis of Fe-doped NiS with different Fe doping quantity

Then, the Fe-$Ni(OH)_2$ precursor 30 mg and amidinothiourea 160 mg were put into a porcelain boat. The sulfur powder was placed at the upstream side and the heating rate was 3 $^oC\ min^{-1}$. After heating at 300 ^oC and maintaining for 1 h in the high-purity nitrogen atmosphere. The molar ratio of Fe to Ni in the precursor of 5%, 10%, and 15% were employed to prepare the final catalyst of Fe-NiS-1, Fe-NiS-2, and Fe-NiS-3, respectively,

Synthesis of pure NiS

The pure NiS was obtained following the same procedure without adding $FeCl_3 \cdot 6H_2O$.

Characterization

The sample was characterized on Bruker D8 advance X-ray diffraction (XRD) with Cu *Kα* radiation source operating at 40 kV and 40 mA at a scanning rate of 5^o min^{-1}. The morphology is examined with an FEI Sirion-200 scanning electron microscope (SEM) and transmission electron microscopy (TEM, Philips, TECNAI 12, Holland). High-resolution TEM and energy-dispersive X-ray spectroscopy (EDS) mapping images were taken under a scanning TEM modal. X-ray

photoelectron spectroscopy (XPS) measurement was carried out on an ECSALAB250Xi spectrometer with an Al K_α radiation source.

Catalytic activity test

(1) Electrochemical measurements

All the electrochemical measurements were carried out by a conventional three-electrode system via a Bio-Logic VSP electrochemical workstation (Bio-Logic Co, France). The working electrode was prepared by coating the catalyst ink over the glassy carbon electrode (3 mm diameter, 0.07 cm^2). The graphite rod and Mercury/mercury oxide electrode (Hg/HgO) were used as the counter and reference electrode, respectively. All tests were carried out at room temperature (around 25 °C). The potential reported at work was converted to the reversible hydrogen electrode, according to the formula: E (RHE) =E (Hg/HgO) + 0.0591*pH + 0.098 V.

The catalyst ink was prepared as follows: The as-obtained catalysts (5 mg) were uniformly dispersed in the mixed solution of 950 μL absolute ethyl alcohol and 50 μL Nafion solution (5 wt.%) through the sonication for 1 h. Then 10 μL of the catalyst ink was pipetted and dropped onto a pre-cleaned glassy carbon and naturally dried. The catalyst loading for the whole catalyst was 0.40 mg cm^{-2}. The glassy carbon electrode was polished, thoroughly cleaned with an alumina slurry of 50 nm, and finally dried at room temperature before use. For OER tests, the linear sweep voltammograms (LSV) and cyclic voltammograms (CV) were measured at a scan rate of 5 mV s^{-1} in 1 M KOH solution. The 1M KOH solution was purged by pure N_2 for approximately 25 min. Fe-containing electrolyte was the purity 1M KOH solution used to test Fe-NiS-2. We can observe that in the EDS there was a little amount of Fe after the OER process, which can indicate that Fe was dissolution into the KOH solution.

(2) Tafel analysis

For the Tafel equation, η = a + b log (j), where η (V) is the overpotential, j (mA cm^{-2}) is the current density, and b (mV dec^{-1}) represented the Tafel slope.

(3) ECSA measurement and calculation

To acquire the electrochemically active surface area (ECSA) of the working electrode, their roughness factor (R_f) should be obtained firstly according to the equation: ECSA = R_f * S, where S was generally equal to the geometric area of the electrode (in this work, S = 0.07 cm^2). The R_f was

determined by the relation $R_f = C_{dl}/40$ based on the double-layer capacitance (C_{dl}) of a smooth metal surface (40 μF cm^{-2}) under the potential of 1.03-1.13 V *vs*. RHE in 1M KOH solution. The scan rates were 20, 40, 60, 80, 100 $mV \cdot s^{-1}$. The C_{dl} was estimated by plotting j at 1.08 V *vs*. RHE (where j is the current density) against the scan rate.

(4) Electrochemical Impedance Measurements

The ohmic resistance used for *iR*-correction was obtained from electrochemical impedance spectroscopy measurements with frequencies ranging from 1000 kHz to 10 mHz with an amplitude of 5 mV.

(5) Stability test and Chronoamperometry measurement

The dynamical stability was tested for many cycles at the constant scan rate of 50 mV s^{-1}. After 1000 and 2000 cycles, the polarization curve at 5 mV s^{-1} was recorded for comparison with the initial curve. To estimate the stability of the catalysts, the chronoamperometry was also performed in 1 M KOH solution at a fixed overpotential of 275 mV for 20 h.

(6) Specific activity and turnover of frequency (TOF) calculation

The specific activity was obtained by normalizing the apparent current to ECSA. The TOF (s^{-1}) for OER can be calculated with the following equation TOF (s^{-1}) = I / (4 * F * n), Where I is the current (A) during linear sweep measurement, F is the Faraday's constant (96485.3 C/mol), n is the number of active sites (mol).

Computational methods

The CASTEP module of the Materials Studio software (Accelrys Inc.) was employed for the quantum chemistry calculations. Perdew−Burke−Ernzerh (PBE) of approximation was selected as the generalized gradient approximation (GGA) method to calculate the exchange-correlation energy. The Broyden−Fletcher−Goldfarb−Shanno (BFGS) scheme was selected as the minimization algorithm. The energy cut-off is 440 eV and the SCF tolerance is 1.0×10^{-6} eV/atom. The optimization is completed when the energy, maximum force, maximum stress and maximum displacement are smaller than 5.0×10^{-6} eV/atom, 0.01 eV/Å, 0.02 G Pa and 5.0×10^{-4} Å, respectively. A vacuum slab exceeding 15 Å was employed in the z direction to avoid the interaction between two periodic units. The model size of NiS is about, a=9.504 Å, b=9.504 Å, c=6.253 Å. Doped Fe is constructed by replacing Ni atoms in NiS model, and the model size is consistent where

the OER progress is studied on the (101) surface. K point is 3×3×4. The model size of NiS_2 is about, a=5.687 Å, b=11.375 Å, c=5.687 Å. Doped Fe is constructed by replacing Ni atoms in NiS_2 model, and the model size is consistent where the OER progress is studied on the (200) surface. K point is 4×2×4. Considering that the main active species in the OER reaction process is NiOOH, the NiOOH/NiS, NiOOH/Fe-NiS and NiOOH/Fe-NiS_2 heterojunction surfaces are constructed based on the NiS, Fe-NiS and Fe-NiS_2 models. The Gibbs free energy of the reaction can be obtained from eqn(1).[1, 2]

$$\Delta G^{*} = \Delta E_{ads} + \Delta E_{ZEP} - T\Delta S \quad (1)$$

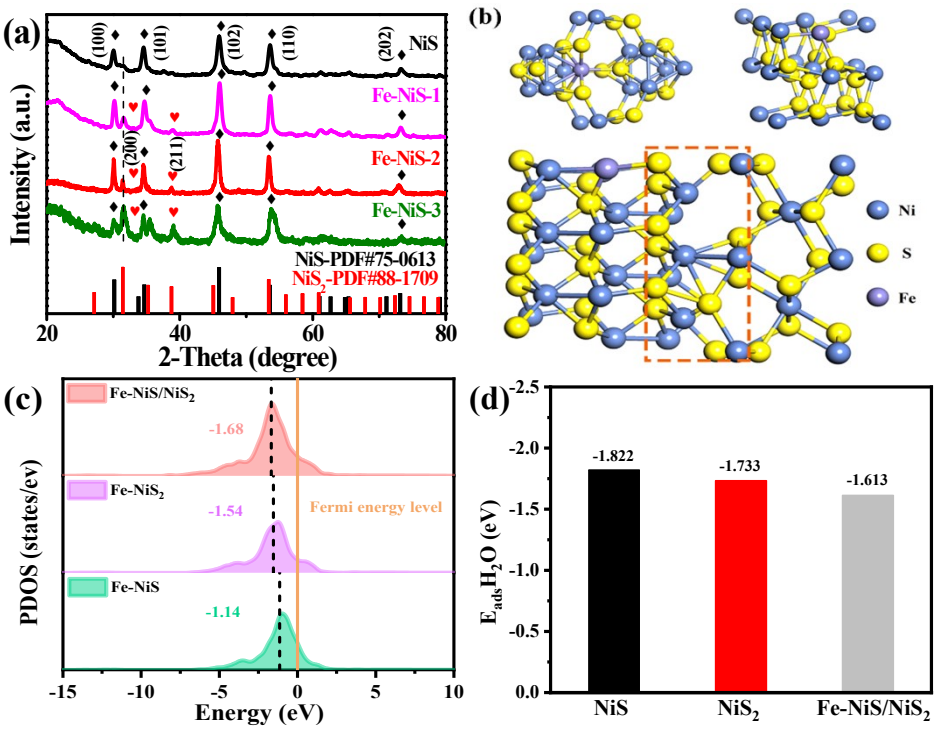

Fig.S1 (a) The X-ray diffraction patterns (XRD) of NiS and different Fe-doped NiS catalysts. (b) The model (and (c) d center of the partial density of states for Fe-doped NiS, Fe-doped NiS_2, and Fe-doped NiS/NiS_2. (d) The adsorption energy of water molecules for NiS, NiS_2 and Fe-NiS/NiS_2.

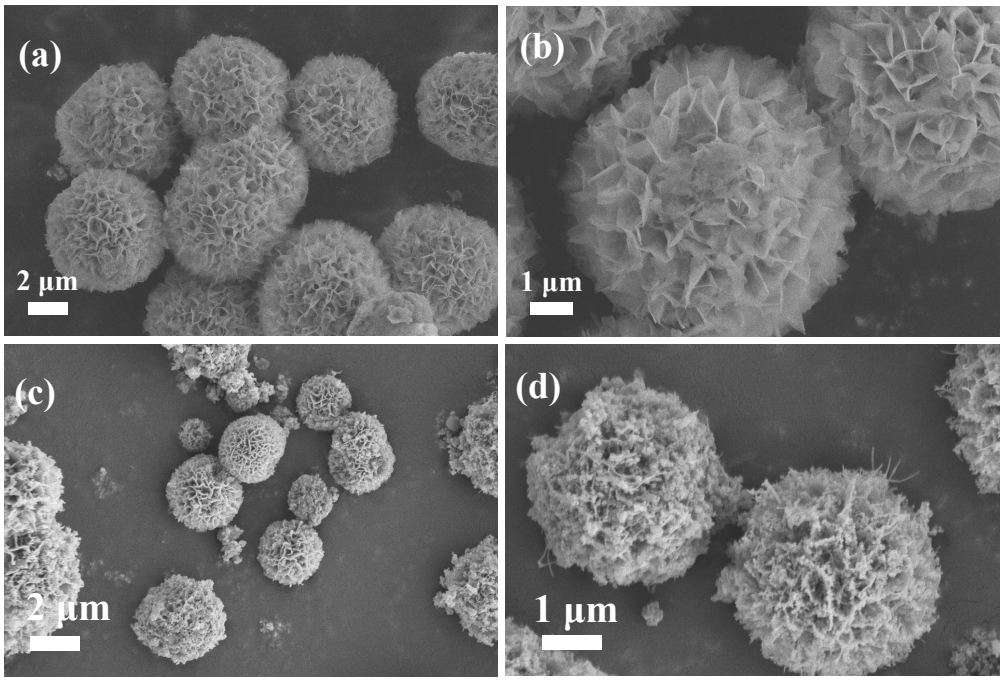

Fig. S2 Scanning electron microscopy (SEM) images of (a-b) Fe-Ni$(OH)_2$ and (c-d) Fe-NiS-2 catalysts.

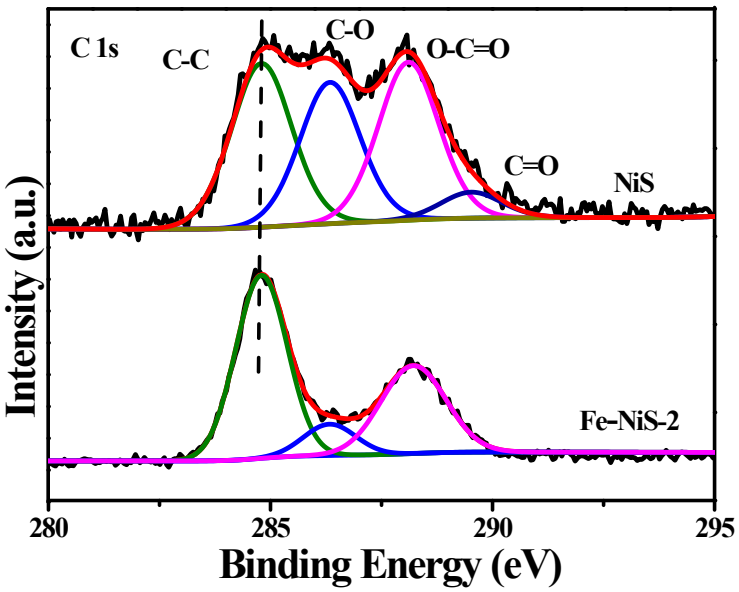

Fig. S3a High-resolution XPS spectrum of C 1s for NiS and Fe-NiS-2 catalysts.

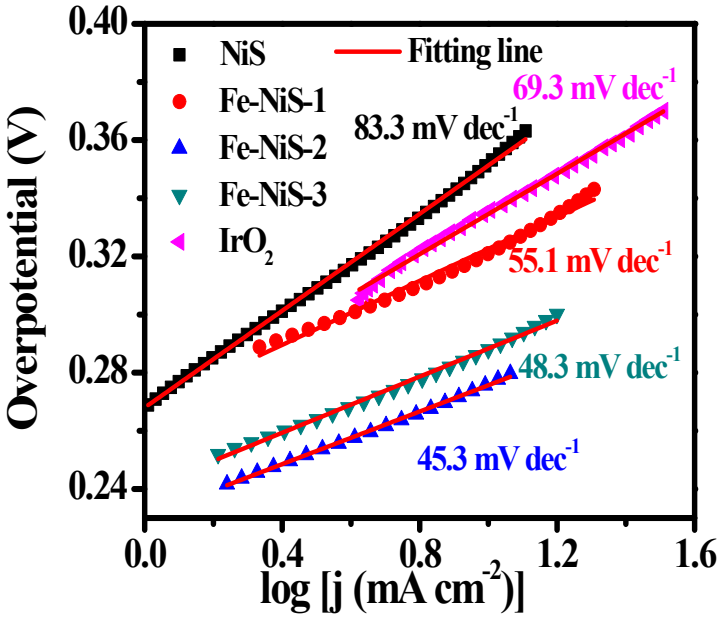

Fig. S3b Tafel slope for NiS and Fe-doped NiS catalysts.

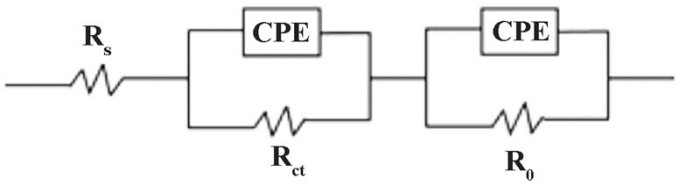

Fig. S4 The equivalent circuit model of EIS analysis. R_s means uncompensated solution resistance, R_{ct} is a charge transfer resistance, R_0 is associated with the contact resistance between the catalysts, and the CPE generally was employed to fit the impedance data by safely treating it as an empirical constant without considering its physical basis. And mostly, it was regarded as the double-layer capacitor from the catalyst/support and catalyst solution.

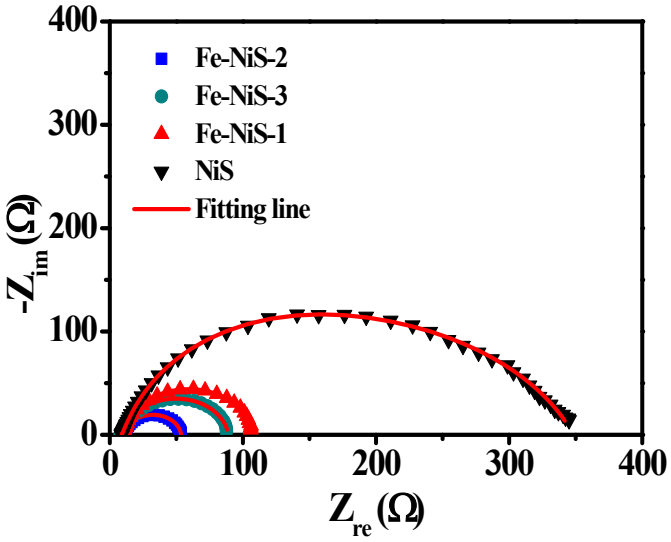

Fig. S5 Nyquist plot of NiS and Fe doped NiS catalysts at the potential of 1.50 V *vs*. RHE.

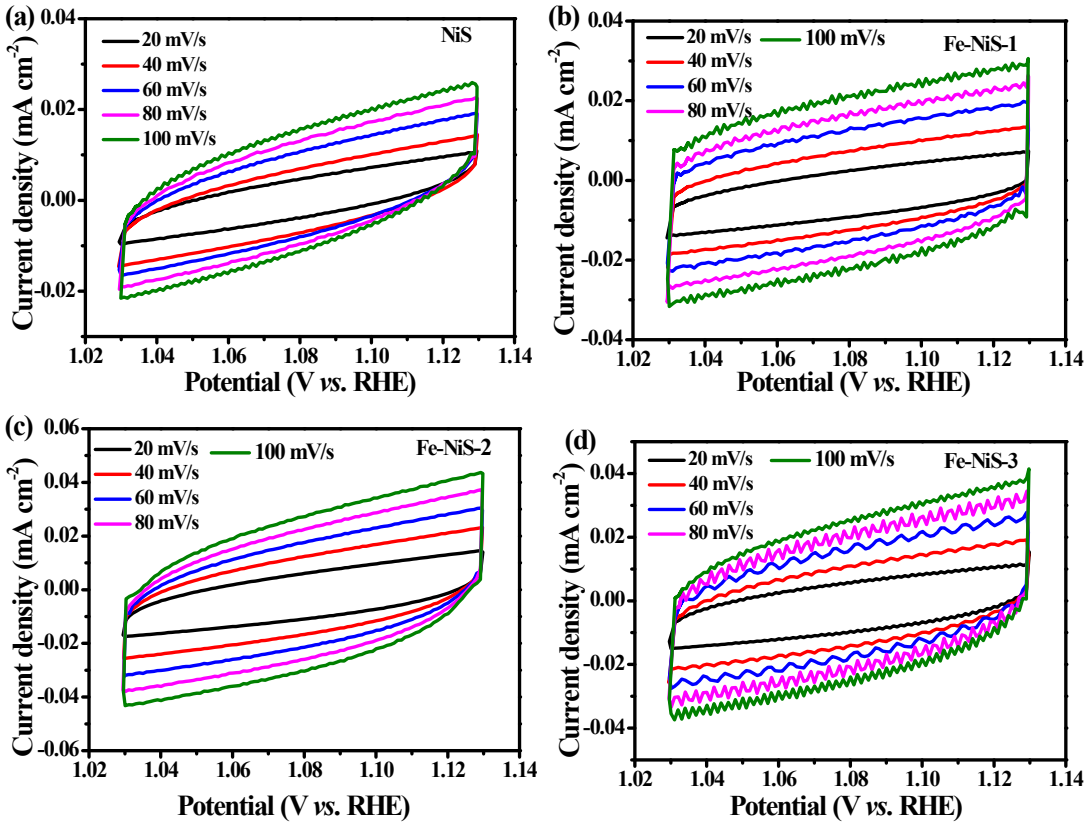

Fig. S6 Cyclic voltammograms of NiS and Fe-doped NiS catalysts in the potential range of 1.03-1.13 V (*vs*. RHE). The capacitive currents as a function of scan rate ($\Delta j = (j_a - j_b)/2$).

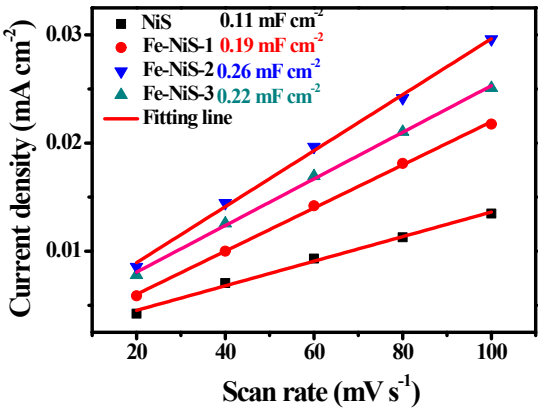

Fig. S7 Linear fitting of current density *vs*. scan rate at 1.08 V range from 1.03 to 1.13 V *vs*. RHE for NiS and Fe-doped NiS in 1 M KOH solution.

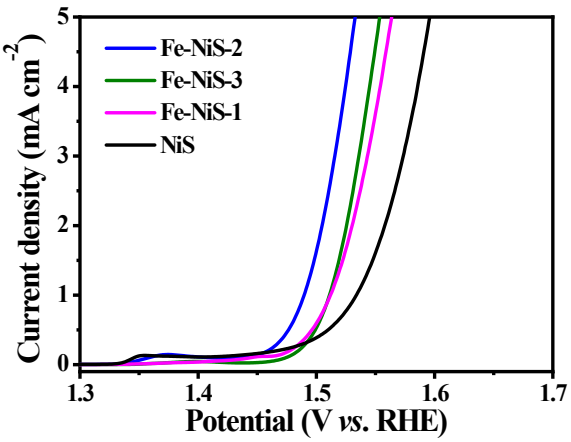

Fig. S8 The specific activity for OER normalized by ECSA.

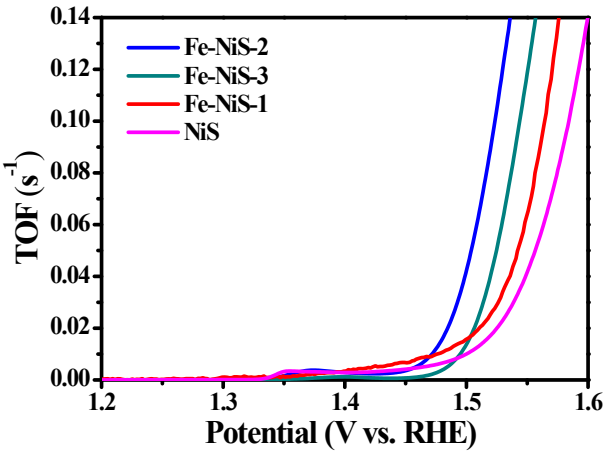

Fig. S9 TOF values of the Fe-NiS-1, Fe-NiS-2, Fe-NiS-3, and NiS as a function of potential.

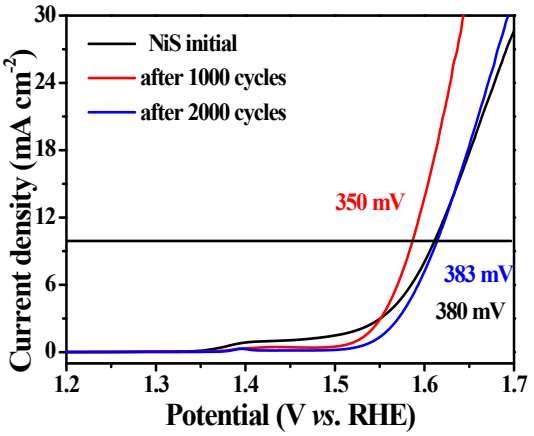

Fig. S10 Polarization curves of freshly configured NiS electrode in Fe containing electrolyte for the initial, after 1000 and after 2000 CV cycles. Condition: Scan rate 5 mV s^{-1}, electrolyte 1 M KOH solution.

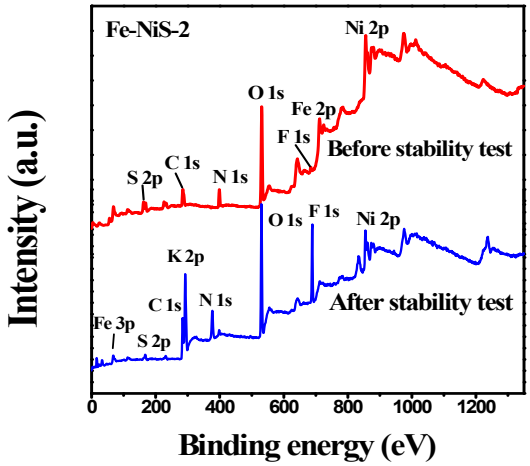

Fig. S11 XPS survey spectra of Fe-NiS-2 before and after the stability test.

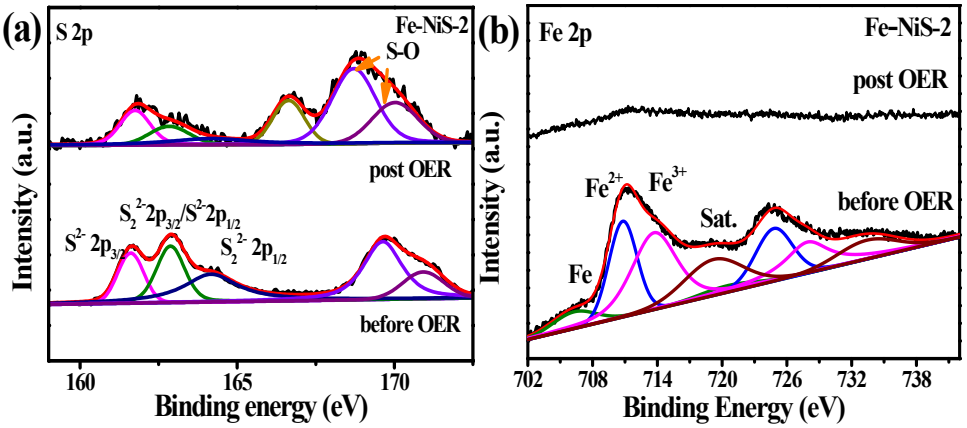

Fig. S12 XPS spectra of Fe-NiS-2 before and post-OER of (a) S 2p and (b) Fe 2p.

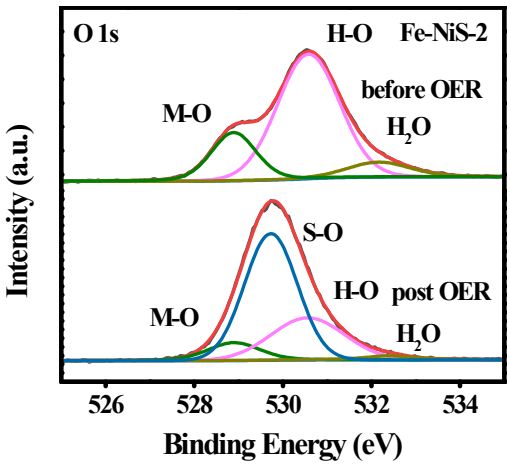

Fig. S13 High-resolution XPS spectrum of O 1s in Fe-NiS-2 before and after OER.

Table S1. Binding energy of the Ni $2p_{3/2}$ and Ni $2p_{1/2}$ components for the Fe-NiS-2 and NiS catalysts.

Catalysts	Ni $2p_{3/2}$		Ni $2p_{1/2}$		Relative content/%
	Peak	Binding energy/eV	Peak	Binding energy/eV	
Fe-NiS-2	Ni(0)	852.6	Ni(0)	870.3	13.3%
	Ni(+2)	855.3	Ni(+2)	873.1	53.6%
	Ni(+3)	857.3	Ni(+3)	875.1	33.1%
NiS	Ni(0)	852.6	Ni(0)	870.3	13.6%
	Ni(+2)	855.6	Ni(+2)	873.4	65.9%
	Ni(+3)	857.6	Ni(+3)	875.4	20.5%

Table S2. Binding energy of the S 2p for the Fe-NiS-2 and NiS catalysts.

Catalysts	S $2p_{3/2}$		S $2p_{1/2}$	
	S^{2-} (eV)	S_2^{2-} (eV)	S^{2-} (eV)	S_2^{2-} (eV)
Fe-Ni-2	161.0	162.3	162.3	163.4
NiS	161.4	/	162.6	/

Table S3. Binding energy of the Fe 2p for the Fe-NiS-2 catalyst.

Catalysts	Fe $2p_{3/2}$		Fe $2p_{1/2}$	
	Peak	**Binding energy/eV**	**Peak**	**Binding energy/eV**
Fe-NiS-2	Fe(0)	706.3	Fe(0)	720.7
	Fe(+2)	710.8	Fe(+2)	725.0
	Fe(+3)	713.7	Fe(+3)	727.9
	Sat.	719.5	Sat.	733.4

Table S4. The comparison of some OER electrocatalysts in alkaline electrolyte.

Catalysts	Electrolytes	supporting electrode	Current density	Overpotential	Ref.
NiS	1M KOH	GCE	10 mA cm^{-2}	350 mV	this work
Fe-NiS-2	1M KOH	GCE	10 mA cm^{-2}	270 mV	this work
Fe-doped NiSe NSs/CNTs	1M KOH	CP	10 mA cm^{-2}	282.7 mV	[3]
Fe-Co_9S_8@SNC	1M KOH	GCE	10 mA cm^{-2}	273 mV	[4]
0.1Fe-NiS/MoS_2	1M KOH	GCE	10 mA cm^{-2}	297 mV	[5]
Fe-NiS/NiS_2	1M KOH	CC	100 mA cm^{-2}	361 mV	[6]
MoC-FeNi@NLC	1M KOH	CP	10 mA cm^{-2}	198 mV	[7]
Ni_2Fe-LDH/$FeNi_2S_4$/NF	1M KOH	NF	100 mA cm^{-2}	240 mV	[8]
FeS/Ni_3S_2@NF	1M KOH	NF	10 mA cm^{-2}	192 mV	[9]
Ni-MOF-Fe-Se-400	1M KOH	GCE	10 mA cm^{-2}	242 mV	[10]
Fe-CoS_2/CoS_2@NC	1M KOH	CP	10 mA cm^{-2}	300 mV	[11]
NiFe-PS	1M KOH	NF	10 mA cm^{-2}	204 mV	[12]
$Co_{0.89}Fe_{11}$O-N	1M KOH	GCE	50 mA cm^{-2}	360 mV	[13]
Fe-MoO_2/MoO_3/ENF	1M KOH	NF	100 mA cm^{-2}	310 mV	[14]
Fe-CoP cage	1M KOH	GCE	10 mA cm^{-2}	300 mV	[15]
$FeNi_3$@NCNT	1M KOH	GCE	10 mA cm^{-2}	264 mV	[16]
Fe-NiCoP/PBA HNCs	1M KOH	GCE	10 mA cm^{-2}	290 mV	[17]
Ni@3FCCO	1M KOH	NF	10 mA cm^{-2}	369 mV	[18]
Fe-NiTe–$Ni_{12}P_5$	1M KOH	NF	50 mA cm^{-2}	303 mV	[19]
Fe-CoO/C	1M KOH	GCE	10 mA cm^{-2}	362 mV	[20]
CoFeP/CoP/CC	1M KOH	CC	10 mA cm^{-2}	240 mV	[21]
FeCoNi-S_2	1M KOH	GCE	10 mA cm^{-2}	280 mV	[22]

Note: GCE as the glassy carbon electrode; CP as the carbon paper; CC as the carbon cloth and NF as the nickel foam.

Table S5. EIS fitting parameters from equivalent circuits of samples during OER process.

Samples	R_s/Ω	R_0/Ω	CPE_1/S s^{-n}	R_{ct}/Ω	CPE/S s^{-n}	Chi quared
NiS	8.9	111.1	6.85E-4	228.4	2.63E-4	1.558E-4
Fe-NiS-1	9.3	11.8	2.94E-4	95.3	1.82E-4	3.470E-4
Fe-NiS-2	9.5	4.1	2.76E-4	47.8	3.64E-3	4.106E-5
Fe-NiS-3	8.6	5.2	1.67E-4	76.1	4.87E-5	4.204E-5

Table S6. ECSA of NiS and Fe-doped NiS catalysts.

Catalysts	ECSA (cm^2)
Fe-NiS-1	0.33
Fe-NiS-2	0.46
Fe-NiS-3	0.39
NiS	0.19

Table S7. TOF of NiS and Fe-doped NiS catalysts at 1.50 V *vs*. RHE.

Catalysts	**TOF (s^{-1})**
Fe-NiS-1	0.016
Fe-NiS-2	0.043
Fe-NiS-3	0.014
NiS	0.010

Table S8. The binding energy of the Ni $2p_{3/2}$ and Ni $2p_{1/2}$ for the Fe-NiS-2 before and post OER.

Catalysts	Ni $2p_{3/2}$		Ni $2p_{1/2}$		Relative content/%
	Peak	Binding energy/eV	Peak	Binding energy/eV	
Fe-NiS-2 before OER	Ni(0)	852.6	Ni(0)	870.3	13.3%
	Ni(+2)	855.3	Ni(+2)	873.1	53.6%
	Ni(+3)	857.3	Ni(+3)	875.1	33.1%
Fe-NiS-2 post OER	Ni(0)	/	Ni(0)	/	0.0%
	Ni(+2)	855.6	Ni(+2)	873.4	52.7%
	Ni(+3)	857.6	Ni(+3)	875.4	47.3%

Table S9. The binding energy of the O 1s spectrum for post-OER of Fe-NiS-2.

Catalysts	O 1s		Relative content/%
	Peak	Binding energy/eV	
Fe-NiS-2 post OER	S-O	830.8	59.0%
	M-O	830.3	12.7%
	H-O	831.5	24.7%
	H_2O	833.5	3.6%

REFERENCES

1 T. Sheng, J. Y. Ye, W. F. Lin and S. G. Sun, *Phys. Chem. Chem. Phys.*, 2017, **19**, 7476-7480.

2 W. Zhong, Y. Liu and D. Zhang, *J. Phys. Chem. C*, 2012, **116**, 2994-3000.

3 K. Chang, D. T. Tran, J. Wang, N. H. Kim and J. H. Lee, *J. Mater. Chem. A*, 2022, **10**, 3102-3111.

4 W. Wang, Y. Yang, Y. Zhao, S. Wang, X. Ai, J. Fang and Y. Liu, *Nano Res.*, 2022, **15**, 872-880.

5 P. Liu, J. Li, J. Yan and W. Song, *Phys. Chem. Chem. Phys.*, 2022, **24**, 8344-8350.

6 X. Zhao, X. Wang, L. Chen, X. Kong, Z. Li, Y. Zhao, Z. Wu, T. Wang, Z. Liu and P. Yang, *J. Electroanal. Chem.*, 2022, **920**, 116630.

7 J. Liu, J. Zhang, H. Zhou, B. Liu, H. Dong, X. Lin and Y. Qin, *J. Colloid Interface Sci.*, 2023, **629**, 822-831.

8 L. Tan, J. Yu, C. Wang, H. Wang, X. Liu, H. Gao, L. Xin, D. Liu, W. Hou and T. Zhan, *Adv. Funct. Mater.*, 2022, **32**, 2200951.

9 H. Li, S. Yang, W. Wei, M. Zhang, Z. Jiang, Z. Yan and J. Xie, *J. Colloid Interface Sci.*, 2022, **608**, 536-548.

10 K. Srinivas, F. Ma, Y. Liu, Z. Zhang, Y. Wu and Y. Chen, *ACS Appl. Mater. Interfaces*, 2022, **14**, 52927-52939.

11 C. Yang, Y.-X. Chang, H. Kang, Y. Li, M. Yan and S. Xu, *Appl. Phys. A*, 2021, **127**, 465.

12 J. Zhang, H. Yu, J. Yang, X. Zhu, M. Hu and J. Yang, *J. Alloys Compd.*, 2022, **924**, 166613.

13 Q. Du, P. Su, Z. Cao, J. Yang, C. A. H. Price and J. Liu, *SM&T*, 2021, **29**, e00293.

14 J. Chen, Q. Zeng, X. Qi, B. Peng, L. Xu, C. Liu and T. Liang, *Int. J. Hydrog.Energy*, 2020, **45**, 24828-24839.

15 J. Y. Xie, Z. Z. Liu, J. Li, L. Feng, M. Yang, Y. Ma, D. P. Liu, L. Wang, Y. M. Chai and B. Dong, *J. Energy Chem.*, 2020, **48**, 328-333.

16 D. Chen, Q. Sun, C. Han, Y. Guo, Q. Huang, W. A. Goddard and J. Qian, *J. Mater. Chem. A*, 2022, **10**, 16007-16015.

17 D. Li, C. Liu, W. Ma, S. Xu, Y. Lu, W. Wei, J. Zhu and D. Jiang, *Electrochim. Acta*, 2021, **367**, 137492.

18 M. Yang, H. Tan, S. Ma, Y. Mi, L. Liu, Z. Zhao, H. Li and D. Xiong, *Nanoscale*, 2023, DOI: 10.1039/D3NR02131A.

19 Y.-J. Tang, Y. Zou and D. Zhu, *J. Mater. Chem. A*, 2022, **10**, 12438-12446.

20 W. Li, M. Li, C. Wang, Y. Wei and X. Lu, *Appl. Surf. Sci.*, 2020, **506**, 144680.

21 D. Jiang, S. Xu, B. Quan, C. Liu, Y. Lu, J. Zhu, D. Tian and D. Li, *J. Colloid Interface Sci.*, 2021, **591**, 67-75.

22 R. He, C. Wang and L. Feng, *Chin. Chem. Lett.*, 2023, **34**, 107241.